Langmuir

Article

pubs.acs.org/Langmuir

H_2O Dissociation-Induced Aluminum Oxide Growth on Oxidized Al(111) Surfaces

Qianqian Liu,[†] Xiao Tong,[‡] and Guangwen Zhou*[,†]

[†]Department of Mechanical Engineering and Multidisciplinary Program in Materials Science and Engineering, State University of New York, Binghamton, New York 13902, United States

[‡]Center for Functional Nanomaterials, Brookhaven National Laboratory, Upton, New York 11973, United States

ABSTRACT: The interaction of water vapor with amorphous aluminum oxide films on Al(111) is studied using X-ray photoelectron spectroscopy to elucidate the passivation mechanism of the oxidized Al(111) surfaces. Exposure of the aluminum oxide film to water vapor results in self-limiting $Al_2O_3/Al(OH)_3$ bilayer film growth via counter-diffusion of both ions, Al outward and OH inward, where a thinner starting aluminum oxide film is more reactive toward H_2O dissociation-induced oxide growth because of the thickness-dependent ionic transport in the aluminum oxide film. The aluminum oxide film exhibits reactivity toward H_2O dissociation in both low-vapor pressure [$p(H_2O) = 1 \times 10^{-6}$ Torr] and intermediate-vapor pressure [$p(H_2O) = 5$ Torr] regimes. Compared to the oxide film growth by exposure to a $p(H_2O)$ of 1×10^{-6} Torr, the exposure to a $p(H_2O)$ of 5 Torr results in the formation of a more open structure of the inner $Al(OH)_3$ layer and a more compact outer Al_2O_3 layer, demonstrating the vapor-pressure-dependent atomic structure in the passivating layer.

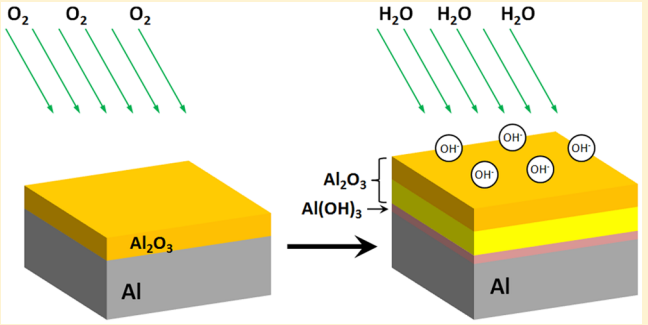

1. INTRODUCTION

The interaction of water with solid surfaces is a topic of great interest for many important processes, such as corrosion, heterogeneous catalysis, environmental chemistry, and biological processes. In particular, the mechanism of the reaction of water with oxide surfaces has been a subject of intensive study because of the widespread use of oxides as catalysts, catalyst supports, and promoters.[1,2] Much of the study has been focused on the surfaces of bulk oxides for understanding the effect of surface structures and surface defects on the dissociation of H_2O molecules. Generally, H_2O adsorbs molecularly at a perfect oxide surface while dissociatively at a nonperfect oxide surface (i.e., surface defect sites).[1−3] More recently, there have been extensive studies of H_2O adsorption on ultrathin aluminum oxide films formed on Al or NiAl surfaces under ultrahigh vacuum (UHV) and non-UHV conditions,[4−9] where the oxide films serve as a surface-science substitute for macroscopically sized single crystals of alumina that typically prohibit the application of surface sensitive tools based on the interactions of matter with charged particles (e.g., electrons and ions). Ultrathin oxide films on metal supports, which can be considered as an "electrically conductive" counterpart of insulating bulk oxides, represent a unique combination of material systems with distinct properties that rely critically on the thickness of the oxide films. It has been suggested that the surface of thin alumina films is inert toward H_2O dissociation under the low-vapor pressure ($<10^{-7}$ Torr) and room-temperature conditions.[10−14] However, under the intermediate pressures (from 10^{-7} to 10^{-1} Torr) and at room temperature, thin alumina films were shown to react with H_2O, which results in additional oxide growth by reaction with subsurface aluminum atoms.[6,8]

Water dissociation for many technologically important processes such as aqueous corrosion and passivation occurs on the surface of a native oxide thin film that is amorphous in nature. Al surfaces are known to develop a protective oxide film upon exposure to oxygen gas at room temperature, and the properties of this oxide layer are extremely important for Al corrosion resistance.[15,16] A detailed understanding of the reactivity of aluminum oxide films with H_2O is necessary for developing protective aluminum oxide films that prevent the metal substrate from dissolution under moisture conditions. H_2O dissociation on aluminum oxide thin films formed on Al or Al alloys results in the growth of the Al oxide film by reacting with Al atoms supplied from the substrate. Because H_2O dissociation-induced oxide growth may require the supply of Al atoms diffusing from the metal substrate through the oxide film to the oxide surface and/or inward diffusion of oxygen-containing species through the oxide film, the thickness of the aluminum oxide film becomes a critical parameter in influencing the surface reactivity of the oxide film toward H_2O dissociation. Alumina exhibits various polymorphs, and

Received: July 27, 2015
Revised: November 6, 2015
Published: November 9, 2015

DOI: 10.1021/acs.langmuir.5b02769
Langmuir 2015, 31, 13117−13126

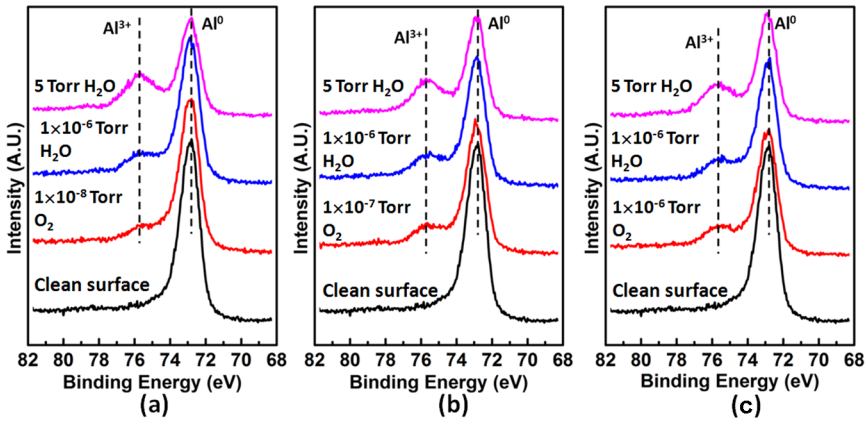

Figure 1. Photoemission spectra of the Al 2p region for a freshly cleaned Al(111) surface (black), oxidized by oxygen exposure (red) at $p(O_2) = 1 \times 10^{-8}$ Torr for 270 min (a), $p(O_2) = 1 \times 10^{-7}$ Torr for 240 min (b), and $p(O_2) = 1 \times 10^{-6}$ Torr for 240 min (c), which are followed by subsequent water vapor exposure $p(H_2O) = 1 \times 10^{-6}$ Torr (blue) and 5 Torr (magenta).

previous study has mainly addressed the effect of the surface structure of crystalline alumina films on H_2O dissociation without much consideration of the effect arising from oxide film thickness.[4,10,12,13,17−20]

The focus of our study is to examine the effect of the thickness of aluminum oxide films on the dissociation of H_2O molecules. We use amorphous aluminum oxide films formed by room-temperature oxidation of Al(111), for which the oxide films have negligible growth and thermal strains, no grain boundaries, and strain-free interfaces with the Al substrate because of the absence of epitaxial oxide growth. This will facilitate addressing the effect of the thickness of the oxide film on H_2O dissociation without possible complication from other effects such as variations in surface structure, grain boundaries, and interfacial strain, which are typically associated with a crystalline oxide film on a metal support. The study of interactions of water vapor with amorphous aluminum oxide films is particularly relevant to understanding the passivation of Al surfaces that occurs typically at low temperatures (e.g., room temperature) with the formation of amorphous aluminum oxide films. In this work, we investigate the dissociation of H_2O on amorphous aluminum oxide films on Al(111) with a controlled thickness of the oxide films. Specifically, we monitor H_2O dissociation-induced oxide growth over a preexisting aluminum oxide film for water vapor dosing at two representative pressures, i.e., 1×10^{-6} and 5 Torr, in the low- and intermediate-pressure regimes. Compared to the extensive study of the oxidation of clean metal surfaces, the fundamental understanding of the effect of a native oxide layer on the subsequent oxidation has been significantly less developed. Our study addresses this issue by examining the surface covered with a preexisting oxide film that resembles the presence of a native oxide layer, which allowed for extraction of the fundamental information about the passivation mechanism of the oxidized surface, including the reaction path, evolution of the atomic structure, and limiting thickness of the oxide film.

2. EXPERIMENTAL SECTION

Our experiments were conducted in an ultrahigh vacuum (UHV) system equipped with an X-ray photoelectron spectroscopy (XPS) SPECS Phoibos 100, MCD-5 analyzer, low-energy electron diffraction (LEED), and an argon ion sputtering gun. The Al(111) single crystal used in the experiment was a top-hat-shaped disc (1 mm in thickness and 8 mm in diameter). The single crystal, purchased from Princeton Scientific Corp., was cut to within 0.1 to the (111) crystallographic orientation and polished to a mirror finish with a purity of 99.9999%. The single crystal was introduced into the UHV chamber (base pressure of 2×10^{-10} Torr) for gas dosing and XPS analysis. The XPS spectra were recorded using a nonmonochromatized Al Kα X-ray source ($h\nu$ = 1486.6 eV) with the electron energy analyzer operated at an anode voltage of 10 kV and an emission current of 30 mA. A ceramic button heater and type-K thermocouple were used for heating and temperature recording, respectively. The Al(111) was treated by cycles of Ar^+ bombardment of 20 min at room temperature with an argon feed gas at a pressure of 5×10^{-5} Torr and an accelerating voltage of 1 kV, and then annealing at 420 °C for 10 min until no O signal could be observed using XPS.

Oxygen gas (99.9999% pure) was directly introduced into the analysis chamber through a variable-pressure leak valve to oxidize the freshly cleaned Al(111) before water vapor dosing. For monitoring H_2O dissociation in the low-pressure regime [i.e., $p(H_2O) = 1 \times 10^{-6}$ Torr], water vapor was directly introduced into the XPS analysis chamber to react with the oxidized Al(111). For H_2O dissociation in the intermediate-pressure regime (i.e., 5 Torr), water vapor dosing was performed in an attached side chamber that permitted in situ transfer of the sample to and from the XPS analysis chamber. Water (18.2 MΩ) was put into a flask and purified with several freeze−pump−thaw cycles before dosing though two separate variable-pressure leak valves, one for the XPS analysis chamber and the other for the side chamber. Gas dosing was conducted at room temperature (25 °C). Ion gauges were used to measure the gas pressures in the different chambers. The effect of the ion gauge sensitivity correction was not accounted for during the pressure measurements because of the minor difference in the gas correction factors for O_2 and H_2O. No carbon contamination was detected by XPS after O_2 and H_2O exposures.

The freshly cleaned Al(111) surface was first oxidized at room temperature by molecular oxygen to a limiting thickness of the aluminum oxide film that depends on oxygen pressure $p(O_2)$.[21−23] In our experiments, oxygen dosing at three pressures [$p(O_2)$], 1×10^{-8}, 1×10^{-7}, and 1×10^{-6} Torr, was performed, which resulted in three different limiting thicknesses of the aluminum oxide films. These oxide films are amorphous in nature, as confirmed by the absence of a LEED pattern, which is also consistent with the transmission electron microscopy characterization of the aluminum oxide film formed under similar oxidation conditions.[15,24−26] After the oxide film was confirmed as having reached its limiting thickness at each $p(O_2)$, the oxidized Al(111) surface was then exposed to water vapor $p(H_2O) = 1 \times 10^{-6}$ and 5 Torr. Al 2p and O 1s spectra were recorded to analyze the oxide film growth induced by O_2 and H_2O exposures. The binding energy scale was frequently calibrated by using the Al 2p peak (72.45 eV) from freshly cleaned Al surfaces. The X-ray flux was constant during our experiment time (several hours), which was confirmed by comparing the Al 2p spectra from freshly cleaned Al surfaces obtained at widely varying times (ranging from several hours to a few days). To

DOI: 10.1021/acs.langmuir.5b02769
Langmuir 2015, 31, 13117−13126

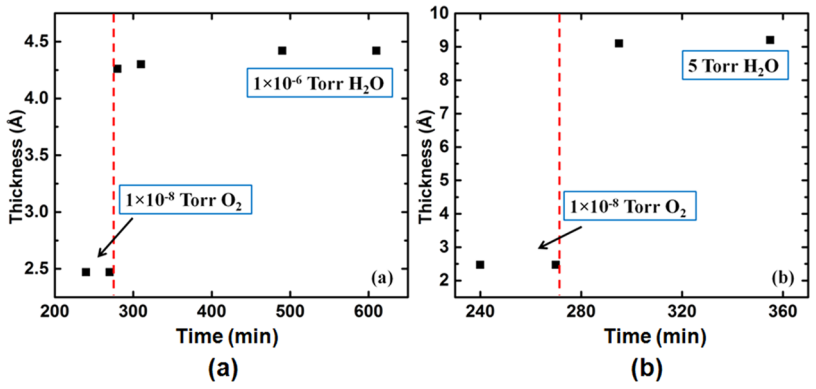

Figure 2. Thickness evolution of the oxide film on Al(111) as a function of oxidation time, where the Al(111) surface was first oxidized to the limiting thickness (~2.5 Å) of the aluminum oxide film by oxygen gas at $p(O_2) = 1 \times 10^{-8}$ Torr for 270 min, which was then followed by exposure to water vapor at (a) $p(H_2O) = 1 \times 10^{-6}$ Torr and (b) $p(H_2O) = 5$ Torr.

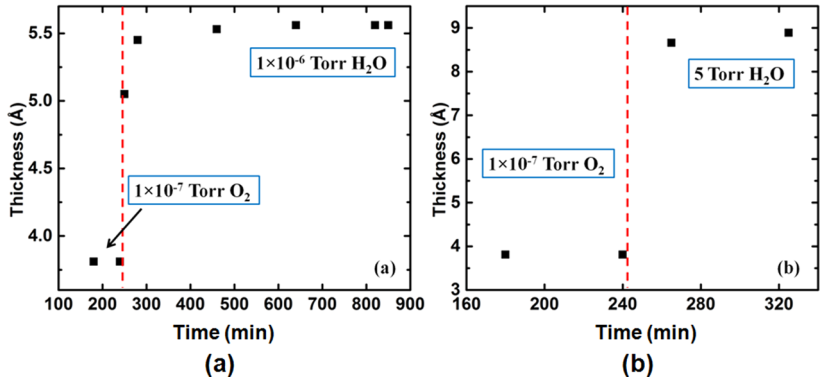

Figure 3. Thickness evolution of the oxide film on Al(111) as a function of oxidation time, where the Al(111) surface was first oxidized to the limiting thickness (~3.8 Å) of the aluminum oxide film by oxygen gas at $p(O_2) = 1 \times 10^{-7}$ Torr for 240 min, which was then followed by exposure to water vapor at (a) $p(H_2O) = 1 \times 10^{-6}$ Torr and (b) $p(H_2O) = 5$ Torr.

minimize the chance of measurement error and to obtain sufficiently reliable XPS data for quantification, the geometry of the X-ray gun, sample, and analyzer was kept constant, and all the XPS spectra were acquired using the same parameters, including pass energy, spot size, lens mode, and dwell time for the energy step. The accuracy of the measurements was also cross-checked using two different methods to quantify the XPS spectra. The equivalent thicknesses of the aluminum oxide films were first determined from the attenuation of the metallic Al 2p spectra in the oxide films with the photoelectron attenuation length for Al_2O_3 (λ = 16.7 ± 0.6 Å)[27,28] by using the formula $d = -\lambda \cos\theta \ln(A/A_o)$, where A is the area of the Al metallic peak after O_2 and H_2O exposures, A_o is the area of the Al metallic peak from the clean surface, λ is the inelastic mean free path, and θ is the angle between the analyzer and the sample surface normal.[29] The thicknesses calculated from the peak attenuation method were also cross-checked using the ratio of the total oxidic Al 2p and metallic Al 2p intensities in a single XPS spectrum of the aluminum oxide film to calculate the oxide film thickness.[30−33] Angle-resolved XPS measurements were made by varying the takeoff angles, i.e., 0°, 30°, and 45°, of the analyzed photoelectrons with respect to the sample surface normal.

3. RESULTS

The clean Al(111) substrate was first oxidized to the limiting thickness of an amorphous aluminum oxide film by filling the analysis chamber with molecular oxygen at room temperature. Oxygen dosing at three different pressures [$p(O_2)$], i.e., 1×10^{-8}, 1×10^{-7}, and 1×10^{-6} Torr, was adopted to form aluminum oxide films that have limiting thicknesses of ~2.5, ~3.8, and ~5.1 Å, respectively. The oxidized Al(111) surfaces were then exposed to water vapor at two representative pressures [$p(H_2O)$], 1×10^{-6} and 5 Torr, for studying H_2O dissociation-induced oxide growth at room temperature. These two vapor pressures were chosen to represent the low- and intermediate-vapor pressure regimes to examine if there is a pressure gap in the reactivity of the amorphous aluminum oxide films toward the dissociation of water molecules.

Figure 1 shows XPS spectra of the Al 2p peaks obtained from the freshly cleaned, O_2-exposed, and subsequently H_2O-exposed Al(111) surfaces. For the clean Al(111) surface, only the metallic Al 2p peak is visible. As shown in Figure 1a, the Al(111) surface was first oxidized by molecular oxygen at $p(O_2) = 1 \times 10^{-8}$ Torr for 270 min to the limiting thickness (~2.5 Å) of the aluminum oxide film, which was confirmed by the saturated intensity of the oxidic Al 2p peak at the higher binding energy. The oxide-covered surface was then exposed to water vapor at $p(H_2O) = 1 \times 10^{-6}$ Torr, which resulted in a decreased intensity of the metallic Al 2p peak and an increased intensity of the oxidic Al 2p peak. This indicates that H_2O molecules dissociated and became incorporated into the oxide film, leading to additional oxide growth. Exposure of the oxidized Al(111) surface to $p(H_2O) = 5$ Torr resulted in a significant decrease in the intensity of the metallic Al 2p and large increase in the intensity of the oxidic Al 2p peak, indicating the growth of a thicker oxide film enabled by the dissociation of water molecules adsorbed at the higher H_2O pressure. A similar trend can be found from the oxidation of the Al(111) first by molecular oxygen at $p(O_2) = 1 \times 10^{-7}$ Torr for 240 min to the limiting thickness (~3.8 Å) of the aluminum

DOI: 10.1021/acs.langmuir.5b02769
Langmuir 2015, 31, 13117−13126

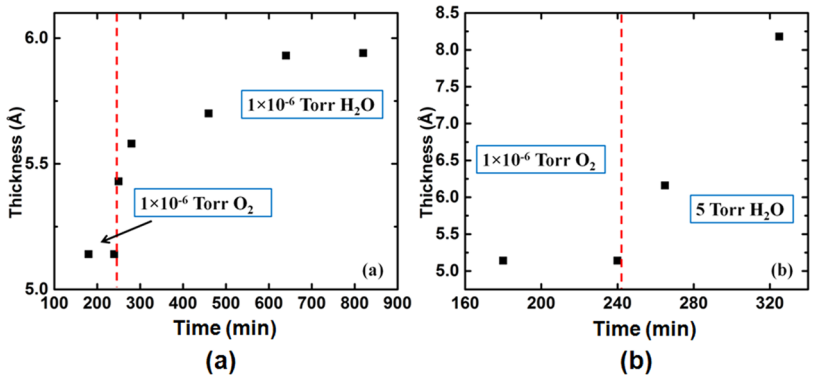

Figure 4. Thickness evolution of the oxide film on Al(111) as a function of oxidation time, where the Al(111) surface was first oxidized to the limiting thickness (~5.1 Å) of the aluminum oxide film by oxygen gas at $p(O_2) = 1 \times 10^{-6}$ Torr for 240 min, which was then exposed to water vapor at (a) $p(H_2O) = 1 \times 10^{-6}$ Torr and (b) $p(H_2O) = 5$ Torr.

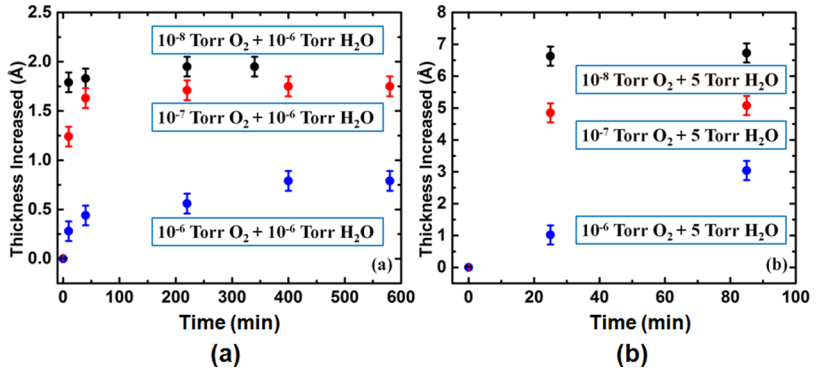

Figure 5. Kinetic curves of the additional oxide film growth upon H_2O exposure to (a) $p(H_2O) = 1 \times 10^{-6}$ Torr and (b) $p(H_2O) = 5$ Torr, where the thicknesses of the starting films formed from the O_2 exposure are subtracted from the total film thickness to highlight the bilayer oxide film growth permitted by H_2O exposure only.

oxide film followed by water vapor exposure $p(H_2O) = 1 \times 10^{-6}$ and 5 Torr (Figure 1b), and the oxidation at $p(O_2) = 1 \times 10^{-6}$ Torr for 240 min to the limiting thickness (~5.1 Å) of the aluminum oxide film followed by water vapor $p(H_2O) = 1 \times 10^{-6}$ and 5 Torr (Figure 1c). It can also be noted from Figure 1 that the positions of both the metallic and oxidic Al 2p peaks remain constant for the O_2 and subsequent H_2O exposures at the different pressures.

Figure 2 shows the kinetic growth curves of the oxide films determined from the attenuation of the metallic Al 2p spectra in the oxide films for the oxidation over a time period extending to approximately 10 h. The O_2 and H_2O exposures were interrupted for XPS measurements. The oxidation started with a clean Al(111) surface at $p(O_2) = 1 \times 10^{-8}$ Torr for 270 min. As shown in Figure 2a, the aluminum oxide layer reached a limiting film thickness of ~2.5 Å at $p(O_2) = 1 \times 10^{-8}$ Torr. Once no further changes in the oxide film thickness were detected, the surface was then exposed to $p(H_2O) = 1 \times 10^{-6}$ Torr, which resulted in additional oxide growth to a limiting film thickness of ~4.4 Å after H_2O exposure for ~220 min. Figure 2b shows the thickness evolution of the oxide film during oxidation at $p(O_2) = 1 \times 10^{-8}$ Torr followed by H_2O exposure at $p(H_2O) = 5$ Torr, which resulted in significant additional growth to a total thickness of ~9.2 Å after H_2O exposure for 85 min.

Figure 3 corresponds to the kinetic curves of the oxide film growth during oxidation of the Al(111) surface at $p(O_2) = 1 \times 10^{-7}$ Torr for 240 min followed by H_2O exposure. The oxidation at $p(O_2) = 1 \times 10^{-7}$ Torr resulted in a thicker limiting thickness (~3.8 Å) of the oxide film [compared to the oxidation at $p(O_2) = 1 \times 10^{-8}$ Torr as shown in Figure 2]. The oxide film grew to a total thickness of ~5.6 Å after subsequent H_2O exposure for 400 min to $p(H_2O) = 1 \times 10^{-6}$ Torr (Figure 3a) and of ~8.9 Å after H_2O exposure for 85 min to $p(H_2O) = 5$ Torr (Figure 3b). Figure 4 shows the thickness evolution of the oxide film from the oxidation of the Al(111) surface at $p(O_2) = 1 \times 10^{-6}$ Torr for 240 min to a limiting thickness of 5.1 Å followed by H_2O exposure. The oxide film grew to a total limiting thickness of ~5.9 Å after exposure for 400 min to $p(H_2O) = 1 \times 10^{-6}$ Torr (Figure 4a). As seen in Figure 4b, the oxide film reached total thicknesses of ~8.2 and 11.6 Å after exposure for 85 and 145 min, respectively, to $p(H_2O) = 5$ Torr, indicating that the oxide film growth did not approach the limiting thickness regime.

The results shown above demonstrate that the amorphous aluminum oxide films formed from the molecular oxygen exposure showed reactivity toward H_2O dissociation at both $p(H_2O) = 1 \times 10^{-6}$ and 5 Torr, which resulted in additional oxide growth. This suggests that no pressure gap exists in the low- and intermediate-pressure regimes of the vapor pressures examined. However, the amount of the additional oxide film growth allowed by the H_2O exposure depends on the thickness of the starting oxide film. Figure 5 shows the thickness evolution of the oxide film upon the H_2O exposure, where the thickness of the starting oxide film is subtracted. Figure 5a corresponds to the oxide growth allowed by exposure to $p(H_2O) = 1 \times 10^{-6}$ Torr. It can be seen that the oxide films had an initial fast growth stage followed by the growth to the

DOI: 10.1021/acs.langmuir.5b02769
Langmuir 2015, 31, 13117−13126

Table 1. Thicknesses of the Oxide Film Formed First by O_2 Exposure Followed by H_2O Exposure[a]

O_2 exposure	1×10^{-8} Torr		1×10^{-7} Torr		1×10^{-6} Torr	
limiting thickness (Å) of the Al_2O_3 film from O_2 exposure	2.5 (3.5)		3.8 (5.0)		5.1 (5.6)	
subsequent H_2O exposure and exposure time	10^{-6} Torr for 220 min	5 Torr for 85 min	10^{-6} Torr for 220 min	5 Torr for 85 min	10^{-6} Torr for 220 min	5 Torr for 85 min
total thickness (Å) of the $[Al_2O_3/Al(OH)_3]$ bilayer film	4.4 (5.9)	9.2 (9.4)	5.5 (6.4)	8.9 (9.0)	5.7 (6.5)	8.2 (7.9)
thickness (Å) of the $Al(OH)_3$ film	0.2 (0.2)	2 (1.9)	0.2 (0.2)	2 (1.9)	0.2 (0.2)	2 (1.9)
thickness (Å) of the Al_2O_3 film permitted by H_2O exposure	1.8 (2.2)	4.7 (4.9)	1.5 (1.2)	2.1 (2.1)	0.4 (0.7)	1.0 (0.4)

[a]Two values are given; the first one is calculated using the attenuation of the metallic Al 2p spectra in the oxide film, while the second value in parentheses is obtained using the ratio of the total oxidic Al 2p and metallic Al 2p intensities in a single XPS spectrum.

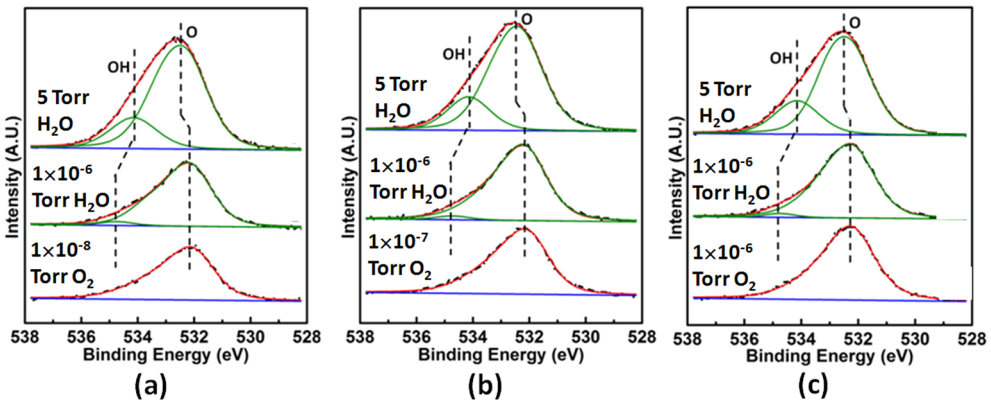

Figure 6. Photoemission spectra of the O 1s peak obtained from the Al(111) surface oxidized at (a) $p(O_2) = 1 \times 10^{-8}$ Torr, (b) $p(O_2) = 1 \times 10^{-7}$ Torr, and (c) $p(O_2) = 1 \times 10^{-6}$ Torr, which were subsequently exposed to water vapor at $p(H_2O) = 1 \times 10^{-6}$ and 5 Torr.

limiting-thickness regime, indicating that the dissociation of H_2O molecules was initially fast and then slowed as the oxide film became thicker. It can be noted that the limiting thickness of the oxide films grown by the H_2O exposure depended inversely on the thickness of the starting oxide film. Figure 5b illustrates the oxide growth induced by exposure to $p(H_2O) = 5$ Torr, and it can be seen that the oxide films grew to much larger thicknesses compared to those at $p(H_2O) = 1 \times 10^{-6}$ Torr. In the case of the thinner starting oxide films [formed from the molecular oxygen exposure at $p(O_2) = 1 \times 10^{-8}$ Torr or $p(O_2) = 1 \times 10^{-7}$ Torr], the oxide films reached their limiting thicknesses of 4.4 and 5.5 Å, respectively, after exposure for 220 min to $p(H_2O) = 1 \times 10^{-6}$ Torr (Figures 2a and 3a). The thicker starting oxide film [formed from the oxidation at $p(O_2) = 1 \times 10^{-6}$ Torr] had a slower rate of oxide growth, and it took ~400 min to reach a limiting thickness of 5.9 Å upon exposure to $p(H_2O) = 1 \times 10^{-6}$ Torr (Figure 4a). A similar trend can be noted from the oxide film growth by exposure to $p(H_2O) = 5$ Torr shown in Figure 5b, where the 2.5 Å thick starting oxide film reached its limiting thickness (9.2 Å) after H_2O exposure for 85 min at $p(H_2O) = 5$ Torr while the 3.8 and 5.1 Å thick starting oxide films have not grown to their limiting thickness regimes after the same amount of H_2O exposure (Figures 2–4). This is particularly obvious for the H_2O exposure of the thickest starting oxide film to $p(H_2O) = 5$ Torr (Figures 4b and 5b), where the oxide film growth did not show any sign of reaching the limiting growth stage. Table 1 summarizes the thicknesses of the oxide films formed from the initial O_2 exposure followed by a fixed amount of H_2O exposure [220 min for $p(H_2O) = 1 \times 10^{-6}$ Torr and 85 min for $p(H_2O) = 5$ Torr] to highlight the effect of the thickness of the starting oxide film on H_2O-induced oxide growth.

The thicknesses of the oxide films shown in Figures 2–5 were determined using the attenuation of the metallic Al^0 2p XPS peak. As seen in the raw XPS data (Figure 1), the difference in the intensity attenuation of the metallic Al^0 2p peak induced by O_2 (or subsequent H_2O) exposure at the different pressures can be discerned visually. Meanwhile, the attenuation of the metallic Al^0 2p peak is correlated well with the increase in the intensity of the oxidic Al^{3+} 2p peak (also seen in Figure 1). The combination of the intensity evolution of both the metallic Al^0 2p and oxidic Al^{3+} 2p peaks is mutually consistent, delivering strong evidence that the behavior of the H_2O-induced oxide film growth shown in Figure 5 is a real feature. Repeated experiments confirmed the oxide growth behavior shown in Figure 5 (where the error bars represent the associated standard deviations determined from the repeated experiments).

Figure 6 illustrates representative photoemission spectra of the O 1s core level region acquired from aluminum oxide films obtained by extended O_2 and H_2O exposures at the different pressures. Figure 6a corresponds to the Al(111) oxidation first at $p(O_2) = 1 \times 10^{-8}$ Torr, followed by exposure to $p(H_2O) = 1 \times 10^{-6}$ and 5 Torr. The O 1s spectra obtained from the O_2 exposure show slight broadening to the high-energy side. In our experiments, a mass spectrometer was used to monitor the gas composition. Tiny amounts of H_2O were present even for O_2 exposure at $p(O_2) = 1 \times 10^{-8}$ Torr. However, their partial pressures were too low to form aluminum hydroxide [i.e., as confirmed by the absence of a detectable oxidic Al^{3+} peak in the H_2O oxidation of the bare Al(111) surface[34]]. The small asymmetries, as seen in the O 1s spectra obtained from the O_2-exposed surface, suggest the presence of a tiny amount of adsorbed OH species on the surface. After the H_2O exposure,

DOI: 10.1021/acs.langmuir.5b02769
Langmuir 2015, 31, 13117–13126

the O 1s spectra became less symmetrical and showed more broadening to the higher-binding energy side. Using the same fitting parameters (e.g., fwhm, L-G%, and asymmetry of the oxidic peak from the O_2 oxidation) does not provide an overall good fitting to the O1 s spectra obtained after the H_2O exposure, and a second peak at a higher binding energy (BE) of 534.8 eV arises. The major peak has the same BE as the O 1s spectra obtained from the O_2-exposed surface and is thus attributed to the O in Al−O bonds in Al_2O_3,[35] and the other peak has a BE of 534.8 eV that is in good agreement with the reported values of OH species and is thus attributed to the O in Al−OH bonds of the aluminum hydroxide [i.e., $Al(OH)_3$].[11,14,33,36] The O 1s spectra obtained from the exposure to $p(H_2O)$ = 5 Torr can be deconvoluted similarly into two peaks, one corresponding to the O in Al_2O_3 with a BE of 532.5 eV and the other corresponding to the O in OH bonds of aluminum hydroxide with a BE of 534.2 eV. It can also be noted that the surface has no undissociated H_2O that has a binding energy of ∼536 eV.[36,37]

Panels b and c of Figure 6 show the O 1s spectra obtained from the oxide films formed at $p(O_2) = 1 \times 10^{-7}$ and 1×10^{-6} Torr followed by exposure to $p(H_2O) = 1 \times 10^{-6}$ and 5 Torr. Similarly, the O 1s spectra from the O_2 exposure have a BE of 532.3 eV, corresponding to the O in Al−O bonds in Al_2O_3. The subsequent H_2O exposure at $p(H_2O) = 1 \times 10^{-6}$ Torr resulted in the O peak with a BE of 532.3 eV corresponding to the O in Al_2O_3 and the OH peak with a BE of 534.8 eV corresponding to the O in $Al(OH)_3$. For the H_2O exposure at $p(H_2O)$ = 5 Torr, the O peak associated with the O in Al_2O_3 shifted to a higher BE of 532.5 eV while the OH peak associated with the O in aluminum $Al(OH)_3$ shifted to a lower BE of 534.2 eV. The positions of the O and OH peaks are also summarized in Table 2. Extensive XPS studies have been reported on the Al−O system to identify the chemical nature of the various O 1s peaks found on the surface, and our analyses indicate that the H_2O exposure leads to chemical shifts ranging from a few tenths of an electronvolt to ∼2 eV. The range of chemical shifts observed in our measurements is in line with the reported values of XPS studies performed on the Al−O system.[9,11,36,38]

Table 2. Binding Energies of O in Al−O Bonds in Al_2O_3 and O in Al−OH Bonds of the Aluminum Hydroxide [i.e., $Al(OH)_3$] Species in the Oxide Films Resulting from O_2 Exposure Followed by H_2O Exposure[a]

	pressure (Torr)	O (eV)	OH (eV)
O_2 exposure	1×10^{-8}	532.3 ± 0.02	–
	1×10^{-7}	532.3 ± 0.02	–
	1×10^{-6}	532.3 ± 0.02	–
subsequent H_2O exposure	1×10^{-6}	532.3 ± 0.02	534.8 ± 0.02
	5	532.5 ± 0.02	534.2 ± 0.02

[a]The estimated errors in the determined position of the peak maximum of the fitted peak are ∼0.02 eV, obtained by averaging over a series of energy values for different oxidation times, and the associated standard deviation is given.

To further elucidate the effect of pressure on oxide growth, we examined the surface oxidation with the sequential O_2 and H_2O exposures at three constant pressures, i.e., O_2 exposure at $p(O_2) = 1 \times 10^{-8}$ Torr followed by H_2O exposure at $p(H_2O) = 1 \times 10^{-8}$ Torr; $p(O_2) = 1 \times 10^{-6}$ Torr followed by $p(H_2O) = 1 \times 10^{-6}$ Torr; and $p(O_2)$ = 5 Torr followed by $p(H_2O)$ = 5 Torr. Shown in Figure 7 are the O 1s spectra obtained from the Al(111) surface oxidized at the three constant pressures, which indicate that the subsequent H_2O dosing resulted in peak broadening to the higher binding energy corresponding to the OH component for the exposures at the two lower pressures (i.e., 1×10^{-8} and 1×10^{-6} Torr), but no distinguishable changes in the O 1s spectra at 5 Torr. This is also constant with the oxide film thicknesses calculated using the attenuation of the metallic Al peak or the intensity ratio of the oxidic/metallic Al peaks. As shown in Table 3, the subsequent H_2O exposure led to slight oxide growth at the two lower pressures but no additional oxide growth at 5 Torr. Comparing these results with those shown in Table 1, we can find that the subsequent H_2O pressure can lead to additional oxide growth even with the same H_2O and O_2 pressure when the initial oxide film is thin. However, if the oxide film resulting from the first O_2 exposure becomes too thick, the subsequent H_2O exposure does not result in any additional oxide growth. This is illustrated from the O_2 exposure at 5 Torr followed by H_2O exposure at 5 Torr. In this case, the surface was completely passivated against H_2O dissociation.

The presence of the OH peak suggests that the H_2O exposures resulted in the growth of an $Al_2O_3/Al(OH)_3$ bilayer film on the Al(111) surface. The relative position of each oxide component within the oxide film can be determined by angle-resolved XPS. Figure 7 shows the spectra of the O 1s peak obtained from the H_2O exposure of the oxidized Al(111) to $p(H_2O) = 1 \times 10^{-6}$ Torr for 220 min and $p(H_2O)$ = 5 Torr for 85 min, where the thickness of the starting aluminum oxide film was ∼5.1 Å. The measurements were performed on the oxide film grown by O_2 exposure at $p(O_2) = 1 \times 10^{-6}$ Torr because of its larger thickness (and thus larger surface/interface separation) compared to those of the oxide films formed at the lower oxygen pressures, which is conducive to the angle-resolved XPS determination of the relative positions of the Al_2O_3 and $Al(OH)_3$ layers. The intensity of the OH peak became weaker, and the O/OH peak intensity ratio increased as the takeoff angle of analyzed photoelectrons was increased from 0° to 45°, as shown in Figure 8. These results indicate that the O component was more surface sensitive than the OH component; i.e., Al_2O_3 formed as an outer layer and $Al(OH)_3$ as an inner layer. The formation of an inner $Al(OH)_3$ layer involves inward transport of OH species from the outer surface to the $Al(OH)_3$/Al interface to form aluminum hydroxide. This is in accordance with the previous study of H_2O-induced aluminum oxide growth on NiAl(100) covered with a preexisting native oxide, which showed that new oxide formation occurred by inward transport of OH anions to the oxide/alloy interface.[9] The formation of such an inner $Al(OH)_3$ layer on the oxidized Al surface (covered with a preexisting oxide film) differs significantly from H_2O oxidation of the bare Al(111) and NiAl(100) surfaces, on which $Al(OH)_3$ formed as an outer layer.[34,39,40]

4. DISCUSSION

The experimental results described above show that the amorphous aluminum oxide films are reactive toward H_2O dissociation (i.e., $2H_2O \rightarrow 2OH_{ads} + H_{2\ gas}$) that results in additional aluminum oxide growth. However, the surface reactivity toward H_2O dissociation depends on the thickness of the starting oxide film. With H_2O exposure at both $p(H_2O)$ = 1×10^{-6} and 5 Torr, a thinner starting aluminum oxide film is more reactive toward H_2O dissociation, as shown in Figure 5

DOI: 10.1021/acs.langmuir.5b02769
Langmuir 2015, 31, 13117−13126

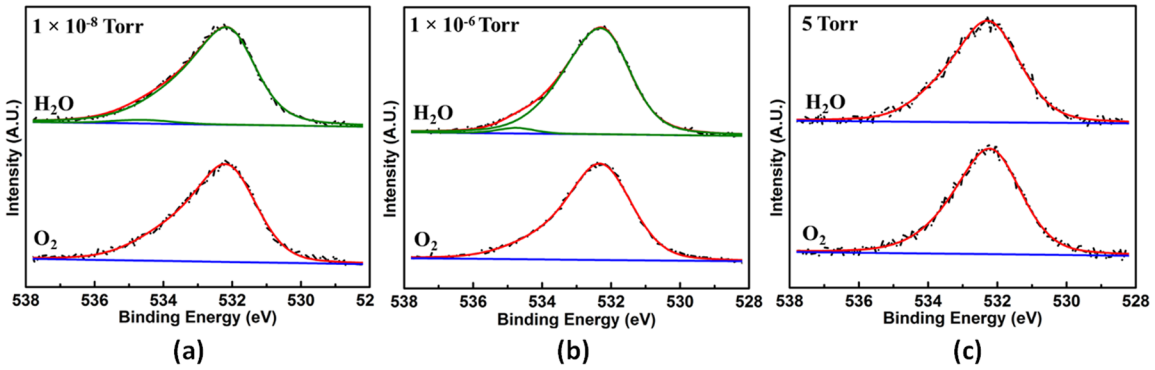

Figure 7. O 1s spectra obtained from the Al(111) surface oxidized by sequential O_2 and H_2O exposures at three constant pressures: (a) 1×10^{-8}, (b) 1×10^{-6}, and (c) 5 Torr.

Table 3. Thicknesses of the Aluminum Oxide Film Formed from the Sequential O_2 and H_2O Exposures at the Constant Pressure[a]

	1×10^{-8} Torr (270 min)	1×10^{-6} Torr (240 min)	5 Torr (90 min)
limiting thickness (Å) of the Al_2O_3 layer from O_2 exposure	2.5 (3.5)	5.1 (5.6)	11.8 (11.9)
subsequent H_2O exposure (and exposure time)	1×10^{-8} Torr (180 min)	1×10^{-6} Torr (220 min)	5 Torr (85 min)
total thickness (Å) of the oxide film by the combined O_2 and H_2O exposure	3.0 (4.3)	5.7 (6.5)	11.8 (11.9)

[a]Two values are given; the first one is calculated using the attenuation of the metallic Al 2p spectra in the oxide film, while the second value in parentheses is obtained using the ratio of the total oxidic Al 2p and metallic Al 2p intensities in a single XPS spectrum.

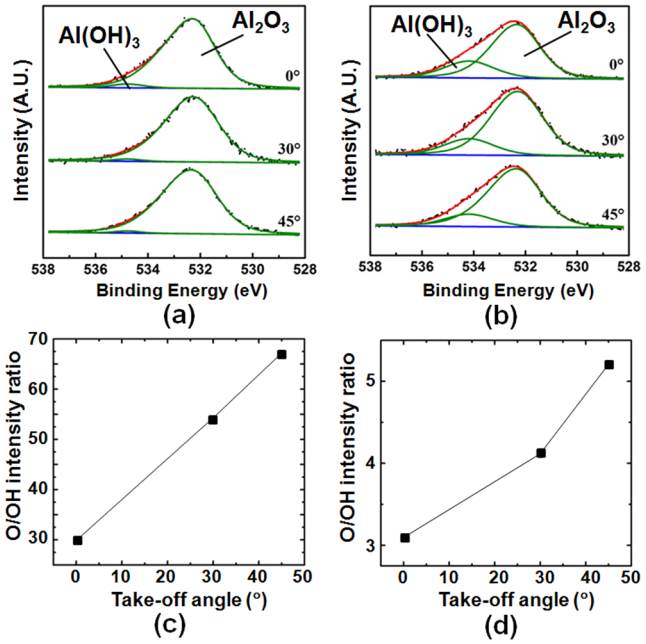

Figure 8. O 1s core level spectra and O/OH intensity ratios measured at takeoff angles of 0°, 30°, and 45° on the Al(111) surface that was first oxidized at $p(O_2) = 1 \times 10^{-6}$ Torr followed by exposure to (a) $p(H_2O) = 1 \times 10^{-6}$ Torr for 220 min (a and c) and $p(H_2O) = 5$ Torr for 85 min (b and d).

and Table 1. Meanwhile, OH species formed by the dissociation of H_2O molecules diffuse through the preexisting Al_2O_3 film to the Al_2O_3/Al interface, which results in the formation of an inner $Al(OH)_3$ layer via the hydration reaction, $Al + 3OH \rightarrow Al(OH)_3$. Such a reaction results in an $Al(OH)_3$/Al_2O_3 bilayer structure as shown schematically in Figure 9.

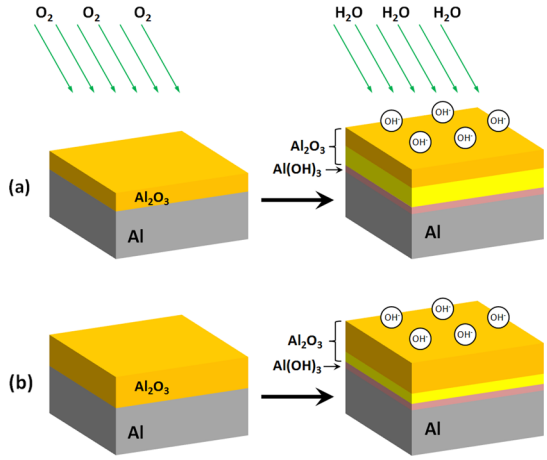

Figure 9. Schematic illustration showing the effect of the thickness of a preexisting Al_2O_3 film on H_2O dissociation-induced oxide growth. (a) A thin starting Al_2O_3 film formed by exposing the Al(111) to molecular oxygen at a low $p(O_2)$ is more reactive toward H_2O dissociation that induces more additional oxide growth than (b) a thicker starting Al_2O_3 film formed at a higher $p(O_2)$, where yellow represents the starting Al_2O_3 film formed from the first O_2 exposure, light yellow the additional Al_2O_3 grown from the subsequent H_2O exposure via the dehydration reaction at the $Al(OH)_3/Al_2O_3$ interface, and pink the $Al(OH)_3$ formed by the hydration reaction via inward diffusion of OH species formed by H_2O dissociation.

Further oxide growth is enabled by the counter diffusion of OH species through the existing Al_2O_3 layer and Al ions from the Al substrate through the $Al(OH)_3$ layer. Because water vapor pressure at the inner interface [i.e., $Al_2O_3/Al(OH)_3$] is low and $Al(OH)_3$ is a metastable phase and a hydrated precursor to Al_2O_3 formation,[41] thickening of the outer Al_2O_3 layer can occur via dehydration decomposition of the $Al(OH)_3$, i.e., $Al(OH)_3 + Al \rightarrow Al_2O_3 + 3H$, at the $Al_2O_3/Al(OH)_3$ interface region. One can note that the total thicknesses of the bilayer oxide films are quite small. These thin thicknesses are less than one unit cell of either Al_2O_3 or $Al(OH)_3$ and do not maintain a periodic atomic structure as a crystal. Because the oxide films

DOI: 10.1021/acs.langmuir.5b02769
Langmuir 2015, 31, 13117−13126

are amorphous, a duplex structure consisting of approximately one atomic layer of Al−OH bonds terminated by a surface layer of Al−O bonds is still physically possible. Even for a crystalline Al_2O_3, thin oxide films with a thickness as thin as ∼1 Å were observed from the oxidation of NiAl(100).[42,43]

The observed limiting thickness behavior of the thin oxide film as shown in Figures 2−4 is consistent with the Cabrera−Mott theory of low-temperature oxidation of metals.[23] Via the operation of this mechanism, the ionic migration is facilitated by a self-generated electric field resulting from the electron tunneling between the Fermi level of the parent metal and acceptor levels of chemisorbed oxygen-containing species at the oxide surface. Because the tunneling current decreases exponentially with an increase in the oxide film thickness, the oxidation essentially stops at a limiting thickness. Our XPS measurements show that a thinner starting oxide film gives a faster rate of oxide formation upon H_2O exposure under the same condition (i.e., temperature and vapor pressure), suggesting that the ionic transport through the existing oxide film controls the H_2O-induced oxide growth. The strength of the self-generated electric field that drives the ionic migration for the oxide growth depends inversely on the thickness of the oxide film, i.e., $E = -V_M/X(t)$, where V_M is the Mott potential and $X(t)$ the oxide film thickness. Meanwhile, the tunneling electron current decreases exponentially with oxide film thickness.[44] Therefore, a thinner starting oxide film results in a stronger self-generated electric field to reduce the energy barrier for ion migration, which thus leads to more H_2O-induced oxide growth. This is in line with our experimental results as shown in Figure 5, where the thinnest starting oxide film leads to the most additional oxide growth after the same amount of H_2O exposure. These XPS measurements demonstrate that the thickness of the oxide film is an important parameter in controlling the dissociation of H_2O molecules via its influence on the self-generated electric field developed across the existing oxide film that drives ion migration through the oxide film for oxide growth. Therefore, a thinner starting aluminum oxide film leads to a faster rate of incorporation of the adsorbed OH species into the oxide, which in turn results in a faster rate of dissociation of adsorbed H_2O molecules. Figure 9 shows a schematic comparison of the effect of the thickness of the starting oxide film on the surface reactivity toward H_2O dissociation-induced oxide growth discussed above.

Our XPS measurements of the evolution of the film thickness upon H_2O exposure showed that H_2O molecules undergo dissociation at both $p(H_2O) = 1 \times 10^{-6}$ and 5 Torr. This indicates that there is no pressure gap in the low- and intermediate-pressure regimes examined here. This is different from the case with ordered alumina films or bulk sapphire, which exhibit a pressure gap for interactions with H_2O molecules at room temperatures. For instance, the surfaces of ordered alumina were found to be inert toward H_2O dissociation for $p(H_2O) < 10^{-7}$ Torr but develop hydroxide for $p(H_2O) > 1$ Torr.[10−14,45] This pressure gap is attributed to the nearest neighbor H-bonding interactions between adjacent H_2O species at higher coverages, which significantly reduce the kinetic barrier to H_2O dissociation.[46] Our results are more in line with the behavior of alumina thin films grown on NiAl surfaces, which are reactive toward dissociation of H_2O at intermediate pressures (e.g., 10^{-7} to 10^{-1} Torr) and room temperatures that results in the growth of a disordered alumina layer initiated at defect sites of the ordered oxide film, although no aluminum hydroxide formation was reported.[4,9] For the oxidation of Al, the oxide films formed at relatively low temperatures ($T < 200$ °C) and low oxygen pressures are amorphous in nature and exhibit a deficiency of Al cations.[24,30,38,47,48] This is consistent with our XPS measurements of the stoichiometry of the oxide films formed under the different oxygen pressures, which is approximately $Al_{2-x}O_3$, where $x \approx 0.24$.[21] Compared to a well-ordered aluminum oxide film, the surface of a nonstoichiometric and amorphous oxide film has a wealth of defective sites that facilitate adsorption and dissociation of H_2O molecules.

While there is no pressure gap in terms of the reaction of the amorphous oxide films with H_2O, the positions of the O and OH peaks show a clear dependence on water vapor pressure. As shown in Figure 6, exposure of all the three preexisting aluminum oxide films to $p(H_2O) = 5$ Torr results in the shift of the OH peak associated with the O in the $Al(OH)_3$ layer to the lower BE while the shift of the O 1s peak associated with the O in the Al_2O_3 layer to the higher BE compared to the exposure to $p(H_2O) = 1 \times 10^{-6}$ Torr. For oxidation at room temperatures and relatively low oxygen pressures, the amorphous aluminum oxide films can be described by a close packing of oxygen anions with Al cations distributed over the octahedral and/or tetrahedral interstices with a deficiency of Al cations.[24,30,38,47,48] In general, the amount of a chemical shift depends on the number of heterogeneous chemical bonds, and shifting to a larger BE can be attributed to a larger average coordination number.[27,34] The chemical shift to the higher BE of the O 1s peak associated with the oxygen in the Al_2O_3 layer reflects the development of a more compact alumina film with an increased coordination number at the higher water vapor pressure [i.e., $p(H_2O) = 5$ Torr].

The peak maxima of the OH peak associated with the growth of the inner $Al(OH)_3$ layer shift to the lower BE at the higher $p(H_2O)$. This can be understood similarly from the evolution of the number of heterogeneous bonds in the $Al(OH)_3$ layer. As shown in Figures 2−4, exposure to $p(H_2O) = 5$ Torr results in a thicker oxide film (thus a smaller self-generated electric field across the oxide film), which slows the inward transport of OH species through the existing oxide film for $Al(OH)_3$ growth. As a result, the $Al(OH)_3$ layer developed at the higher $p(H_2O)$ has a structure (e.g., more dangling bonds because of the deficiency of OH ions) more open than that of the oxide film formed under $p(H_2O) = 1 \times 10^{-6}$ Torr. This results in a chemical shift to the smaller binding energy of the OH peak. Therefore, the evolution of the atomic structure of the $Al(OH)_3$ layer depends on $p(H_2O)$, and a higher $p(H_2O)$ results in a more open structure of the $Al(OH)_3$ layer. These results show that there is a pressure gap that induces variations in the atomic structure of the oxide film during the water vapor exposure; i.e., the $Al_2O_3/Al(OH)_3$ bilayer film formed in the intermediate vapor pressure regime has a more open structure of the inner $Al(OH)_3$ layer while a more compact structure of the outer Al_2O_3 layer compared to that of the low-pressure regime. However, one can note from Figure 1 that the position of the oxidic Al 2p peak does not change for the O_2 and H_2O exposures at the different pressures, suggesting that the overall concentration of Al cations in the entire $Al_2O_3/Al(OH)_3$ bilayer system remains relatively the same.

It is noted from Figure 6 that the O 1s peak associated with the oxygen in Al_2O_3 for water vapor exposure at $p(H_2O) = 1 \times 10^{-6}$ Torr does not show a noticeable BE shift from that of the preexisting Al_2O_3 films but shifts to a higher BE for water vapor exposure at $p(H_2O) = 5$ Torr. This difference can be attributed

DOI: 10.1021/acs.langmuir.5b02769
Langmuir 2015, 31, 13117−13126

to the amount of additional oxide growth permitted by the H_2O exposure at the two water vapor pressures. As shown in Table 1, the additional oxide growth induced by the water vapor exposure at $p(H_2O) = 1 \times 10^{-6}$ Torr is much smaller than that at $p(H_2O) = 5$ Torr. Therefore, the chemical environment in the outer Al_2O_3 is still dominated by the preexisting Al_2O_3 film because of the small amount of additional oxide growth at $p(H_2O) = 1 \times 10^{-6}$ Torr, while it evolves to a more compact atomic structure for the significant additional oxide growth at $p(H_2O) = 5$ Torr.

5. CONCLUSIONS

We report a comparative study of the room-temperature H_2O dissociation-induced oxide growth on the Al(111) surface covered with a preexisting amorphous aluminum oxide film. It is shown that exposing the oxidized Al(111) surface to H_2O results in the formation of an $Al_2O_3/Al(OH)_3$ bilayer film with $Al(OH)_3$ as the inner layer. The surface reactivity of the aluminum oxide film toward H_2O dissociation shows a dependence on the thickness of the starting oxide films; i.e., a thinner aluminum oxide film is more reactive toward H_2O dissociation. This thickness-dependent surface reactivity for H_2O dissociation-induced oxide growth is attributed to the thickness-dependent transport of OH and Al ions in the oxide film. Although there is no pressure gap for the reactions of the oxide films with H_2O in the low- and intermediate-pressure regimes due to the defective and amorphous nature of the oxide films, the atomic structure of the oxide films formed shows a dependence on water vapor pressure. H_2O exposure at 5 Torr results in a more open structure of the inner $Al(OH)_3$ layer and a more compact outer Al_2O_3 layer compared to the oxide film formed at $p(H_2O) = 1 \times 10^{-6}$ Torr. However, the overall Al concentration in the entire $Al(OH)_3/Al_2O_3$ bilayer remains relatively constant for the different vapor pressures.

AUTHOR INFORMATION

Corresponding Author

*E-mail: gzhou@binghamton.edu.

Notes

The authors declare no competing financial interest.

ACKNOWLEDGMENTS

We acknowledge the support from the National Science Foundation via CAREER Award Grant CMMI-1056611. Research in part was conducted in the Center for Functional Nanomaterials, Brookhaven National Laboratory, which is supported by the U.S. Department of Energy, Office of Basic Energy Sciences, under Contract DE-AC02-98CH10886.

REFERENCES

(1) Thiel, P. A.; Madey, T. E. The Interaction of Water with Solid Surfaces: Fundamental Aspects. *Surf. Sci. Rep.* **1987**, *7*, 211−385.

(2) Henderson, M. A. The Interaction of Water with Solid Surfaces: Fundamental Aspects Revisited. *Surf. Sci. Rep.* **2002**, *46*, 1−308.

(3) Layman, K. A.; Hemminger, J. C. Determination of Surface OH Acidity from the Formation of Acid/Base Complexes on Ultrathin Films of γ-Al_2O_3 on NiAl(100). *J. Catal.* **2004**, *222*, 207−213.

(4) Kelber, J.; Magtoto, N.; Vamala, C.; Jain, M.; Jennison, D. R.; Schultz, P. A. Reactivities of Ultrathin Alumina Films Exposed to Intermediate Pressures of H_2O: Substrate-Mediated Mechanism for Growth and Loss of Surface Order. *Surf. Sci.* **2007**, *601*, 3464−3471.

(5) Kelber, J. A. Alumina Surfaces and Interfaces under Non-Ultrahigh Vacuum Conditions. *Surf. Sci. Rep.* **2007**, *62*, 271−303.

(6) Qin, F.; Magtoto, N. P.; Kelber, J. A. H_2O-Induced Instability of $Al_2O_3/Ni_3Al(110)$ and $Al_2O_3/Ni_3Al(111)$ Thin Films under Non-UHV Conditions. *Surf. Sci.* **2004**, *565*, L277−L282.

(7) Ozensoy, E.; Szanyi, J.; Peden, C. H. F. Interaction of Water with Ordered θ-Al_2O_3 Ultrathin Films Grown on NiAl(100). *J. Phys. Chem. B* **2005**, *109*, 3431−3436.

(8) Maurice, V.; Frémy, N.; Marcus, P. Hydroxylation-Induced Modifications of the Al_2O_3/NiAl(001) Surface at Low Water Vapour Pressure. *Surf. Sci.* **2005**, *581*, 88−104.

(9) Maurice, V.; Bennour, I. s.; Zanna, S.; Klein, L. H.; Marcus, P. Modifications and Growth Mechanisms of Ultrathin Aluminum Oxide Films on NiAl in Water. *J. Phys. Chem. C* **2010**, *114*, 7132−7140.

(10) Libuda, J.; Frank, M.; Sandell, A.; Andersson, S.; Brühwiler, P. A.; Bäumer, M.; Mårtensson, N.; Freund, H. J. Interaction of Rhodium with Hydroxylated Alumina Model Substrates. *Surf. Sci.* **1997**, *384*, 106−119.

(11) Garza, M.; Magtoto, N. P.; Kelber, J. A. Characterization of Oxidized $Ni_3Al(110)$ and Interaction of the Oxide Film with Water Vapor. *Surf. Sci.* **2002**, *519*, 259−268.

(12) Liu, P.; Kendelewicz, T.; Brown, G. E., Jr; Nelson, E. J.; Chambers, S. A. Reaction of Water Vapor with α-$Al_2O_3(0001)$ and α-$Fe_2O_3(0001)$ Surfaces: Synchrotron X-ray Photoemission Studies and Thermodynamic Calculations. *Surf. Sci.* **1998**, *417*, 53−65.

(13) Elam, J. W.; Nelson, C. E.; Cameron, M. A.; Tolbert, M. A.; George, S. M. Adsorption of H_2O on a Single-Crystal α-Al2O3(0001) Surface. *J. Phys. Chem. B* **1998**, *102*, 7008−7015.

(14) Niu, C.; Shepherd, K.; Martini, D.; Tong, J.; Kelber, J. A.; Jennison, D. R.; Bogicevic, A. Cu Interactions with α-$Al_2O_3(0001)$: Effects of Surface Hydroxyl Groups Versus Dehydroxylation by Ar-Ion Sputtering. *Surf. Sci.* **2000**, *465*, 163−176.

(15) Reichel, F.; Jeurgens, L. P. H.; Richter, G.; Mittemeijer, E. J. Amorphous Versus Crystalline State for Ultrathin Al_2O_3 Overgrowths on Al Substrates. *J. Appl. Phys.* **2008**, *103*, 093515.

(16) Doherty, P. E.; Davis, R. S. Direct Observation of the Oxidation of Aluminum Single-Crystal Surfaces. *J. Appl. Phys.* **1963**, *34*, 619−628.

(17) Tzvetkov, G.; Zubavichus, Y.; Koller, G.; Schmidt, T.; Heske, C.; Umbach, E.; Grunze, M.; Ramsey, M. G.; Netzer, F. P. Growth of H_2O Layers on an Ultra-Thin Al_2O_3 Film: from Monomeric Species to Ice. *Surf. Sci.* **2003**, *543*, 131−140.

(18) Coustet, V.; Jupille, J. High-Resolution Electron-Energy-Loss Spectroscopy of Isolated Hydroxyl Groups on α-$Al_2O_3(0001)$. *Surf. Sci.* **1994**, *307*−*309*, 1161−1165.

(19) Nelson, C. E.; Elam, J. W.; Cameron, M. A.; Tolbert, M. A.; George, S. M. Desorption of H_2O from a Hydroxylated Single-Crystal α-$Al_2O_3(0001)$ Surface. *Surf. Sci.* **1998**, *416*, 341−353.

(20) Chen, J. G.; Crowell, J. E.; Yates, J. T. Assignment of a Surface Vibrational Mode by Chemical Means: Modification of the Lattice Modes of Al_2O_3 by a Surface Reaction with H_2O. *J. Chem. Phys.* **1986**, *84*, 5906−5909.

(21) Cai, N.; Zhou, G.; Müller, K.; Starr, D. E. Tuning the Limiting Thickness of a Thin Oxide Layer on Al(111) with Oxygen Gas Pressure. *Phys. Rev. Lett.* **2011**, *107*, 035502.

(22) Cai, N.; Zhou, G.; Müller, K.; Starr, D. E. Effect of Oxygen Gas Pressure on the Kinetics of Alumina Film Growth during the Oxidation of Al(111) at Room Temperature. *Phys. Rev. B: Condens. Matter Mater. Phys.* **2011**, *84*, 125445.

(23) Cai, N.; Zhou, G.; Müller, K.; Starr, D. E. Temperature and Pressure Dependent Mott Potentials and their Influence on Self-Limiting Oxide Film Growth. *Appl. Phys. Lett.* **2012**, *101*, 171605.

(24) Snijders, P. C.; Jeurgens, L. P. H.; Sloof, W. G. Structure of Thin Aluminium-Oxide Films Determined from Valence Band Spectra Measured Using XPS. *Surf. Sci.* **2002**, *496*, 97−109.

(25) Kuznetsova, A.; Yates, J. T.; Zhou, G.; Yang, J. C.; Chen, X. Making a Superior Oxide Corrosion Passivation Layer on Aluminum Using Ozone. *Langmuir* **2001**, *17*, 2146−2152.

(26) Kuznetsova, A.; Popova, I.; Zhukov, V.; Yates, J. T.; Zhou, G.; Yang, J. C.; Chen, X. Making Superior Corrosion Resistant Aluminum Oxide Films Using Ozone-Electrochemical and Electron Microscopy Studies. *J. Vac. Sci. Technol., A* **2001**, *19*, 1971−1976.

DOI: 10.1021/acs.langmuir.5b02769
Langmuir 2015, 31, 13117−13126

(27) Graupner, H.; Hammer, L.; Heinz, K.; Zehner, D. M. Oxidation of Low-Index FeAl Surfaces. *Surf. Sci.* **1997**, *380*, 335−351.
(28) Battye, F. L.; Jenkin, J. G.; Liesegang, J.; Leckey, R. C. G. Photoelectron Determination of the Attenuation of Low-Energy Electrons in Al_2O_3. *Phys. Rev. B* **1974**, *9*, 2887−2893.
(29) Tanuma, S.; Powell, C. J.; Penn, D. R. Calculations of Electron Inelastic Mean Free Paths. V. Data for 14 Organic Compounds over the 50−2000 eV Range. *Surf. Interface Anal.* **1994**, *21*, 165−176.
(30) Jeurgens, L. P. H.; Sloof, W. G.; Tichelaar, F. D.; Mittemeijer, E. J. Growth Kinetics and Mechanisms of Aluminum-Oxide Films Formed by Thermal Oxidation of Aluminum. *J. Appl. Phys.* **2002**, *92*, 1649−1656.
(31) Jeurgens, L. P. H.; Sloof, W. G.; Tichelaar, F. D.; Borsboom, C. G.; Mittemeijer, E. J. Determination of Thickness and Composition of Aluminium-Oxide Overlayers on Aluminium Substrates. *Appl. Surf. Sci.* **1999**, *144−145*, 11−15.
(32) Yi, C.-W.; Szanyi, J. $BaO/Al_2O_3/NiAl(110)$ Model NO_x Storage Materials: The Effect of BaO Film Thickness on the Amorphous-to-Crystalline $Ba(NO_3)_2$ Phase Transition. *J. Phys. Chem. C* **2009**, *113*, 716−723.
(33) Chen, C.; Splinter, S. J.; Do, T.; McIntyre, N. S. Measurement of Oxide Film Growth on Mg and Al Surfaces over Extended Periods Using XPS. *Surf. Sci.* **1997**, *382*, L652−L657.
(34) Cai, N.; Qin, H.; Tong, X.; Zhou, G. Growth of Ultrathin Amorphous Alumina Films during the Oxidation of NiAl(100). *Surf. Sci.* **2013**, *618*, 20−26.
(35) Kishi, K.; Ikeda, S. X-Ray Photoelectron Spectroscopic Study for the Reaction of Evaporated Iron with O_2 and H_2O. *Bull. Chem. Soc. Jpn.* **1973**, *46*, 341−345.
(36) Deng, X.; Herranz, T.; Weis, C.; Bluhm, H.; Salmeron, M. Adsorption of Water on Cu_2O and Al_2O_3 Thin Films. *J. Phys. Chem. C* **2008**, *112*, 9668−9672.
(37) Yamamoto, S.; Andersson, K.; Bluhm, H.; Ketteler, G.; Starr, D. E.; Schiros, T.; Ogasawara, H.; Pettersson, L. G. M.; Salmeron, M.; Nilsson, A. Hydroxyl-Induced Wetting of Metals by Water at Near-Ambient Conditions. *J. Phys. Chem. C* **2007**, *111*, 7848−7850.
(38) Jeurgens, L. P. H.; Sloof, W. G.; Tichelaar, F. D.; Mittemeijer, E. J. Composition and Chemical State of the Ions of Aluminium-Oxide Films Formed by Thermal Oxidation of Aluminium. *Surf. Sci.* **2002**, *506*, 313−332.
(39) Cai, N.; Liu, Q.; Tong, X.; Zhou, G. X-ray Photoelectron Spectroscopy Study of the Passivation of NiAl(100) by Water Vapor. *Langmuir* **2014**, *30*, 774−783.
(40) Cai, N.; Zhou, G.; Müller, K.; Starr, D. E. Comparative Study of the Passivation of Al(111) by Molecular Oxygen and Water Vapor. *J. Phys. Chem. C* **2013**, *117*, 172−178.
(41) Digne, M.; Sautet, P.; Raybaud, P.; Toulhoat, H.; Artacho, E. Structure and Stability of Aluminum Hydroxides: A Theoretical Study. *J. Phys. Chem. B* **2002**, *106*, 5155−5162.
(42) Qin, H.; Chen, X.; Li, L.; Sutter, P. W.; Zhou, G. Oxidation-Driven Surface Dynamics on NiAl(100). *Proc. Natl. Acad. Sci. U. S. A.* **2015**, *112*, E103−E109.
(43) Qin, H.; Zhou, G. The Formation of Double-Row Oxide Stripes during the Initial Oxidation of NiAl(100). *J. Appl. Phys.* **2013**, *114*, 083513.
(44) Cabrera, N.; Mott, N. F Theory of the Oxidation of Metals. *Rep. Prog. Phys.* **1949**, *12*, 163.
(45) Eng, P. J.; Trainor, T. P.; Brown, G. E., Jr.; Waychunas, G. A.; Newville, M.; Sutton, S. R.; Rivers, M. L. Structure of the Hydrated α-Al_2O_3 (0001) Surface. *Science* **2000**, *288*, 1029−1033.
(46) Hass, K. C.; Schneider, W. F.; Curioni, A.; Andreoni, W. The Chemistry of Water on Alumina Surfaces: Reaction Dynamics from First Principles. *Science* **1998**, *282*, 265−268.
(47) Jeurgens, L. P. H.; Sloof, W. G.; Tichelaar, F. D.; Mittemeijer, E. J. Thermodynamic Stability of Amorphous Oxide Films on Metals: Application to Aluminum Oxide Films on Aluminum Substrates. *Phys. Rev. B: Condens. Matter Mater. Phys.* **2000**, *62*, 4707−4719.
(48) Jeurgens, L. P. H.; Sloof, W. G.; Tichelaar, F. D.; Mittemeijer, E. J. Structure and Morphology of Aluminium-Oxide Films Formed by Thermal Oxidation of Aluminium. *Thin Solid Films* **2002**, *418*, 89−101.

DOI: 10.1021/acs.langmuir.5b02769
Langmuir 2015, 31, 13117−13126